LHCb internal note TRAC–98/060
HERA–B internal note 98-149
HERA–B Inner Tracker 98-020
October 6, 1998

Operation of a large GEM-MSGC detector in a high intensity hadronic test beam using fully pipelined readout electronics

H.-B. Dreis, F. Eisele, M. Feuerstack-Raible, M. Gerlowski, W. Gradl, S. Hausmann, M. Hildebrandt, S. Löchner, K. Müller, C. Richter, B. Schmidt, U. Straumann[1], S. Wunderlich, M. Ziegler
Physikalisches Institut Universität Heidelberg

S. Keller, A. Lange, U. Werthenbach, G. Zech, T. Zeuner
Universität-Gesamthochschule Siegen

P. Robmann, P. Truöl, T. Walter
Physik Institut Universität Zürich

In a recent test beam experiment at PSI a new tracking device for very high particle fluxes consisting of a low gain micro strip gas chamber (MSGC) combined with a gas electron multiplier (GEM) foil has been run under beam conditions similar to those foreseen in the HERA-B experiment [1], where such devices are being installed for the inner tracker. They are also being evaluated for the LHCb experiment [2]. In both detectors very high, mainly hadronic particle densities (up to 10^4 mm^{-2}sec^{-1}) are expected, while the momentum resolution of the magnetic spectrometers foreseen in the two experiments is limited by multiple scattering. Also photon conversions represent a significant background source and therefore a minimal thickness in terms of radiation length is important, while position resolution requirements are moderate (typically 300 μm pitch is sufficient).

This paper describes the detailed construction of this novel detector, the test beam configuration and some of the data taken using the full HERA-B readout electronics.

1 Experimental setup

1.1 Beam

Previous experience [8, 9] has shown that gas multiplication detectors perform significantly different in high intensity hadronic beams than in the usual laboratory setups with nuclear

[1]corresponding author, email: strauman@physi.uni-heidelberg.de

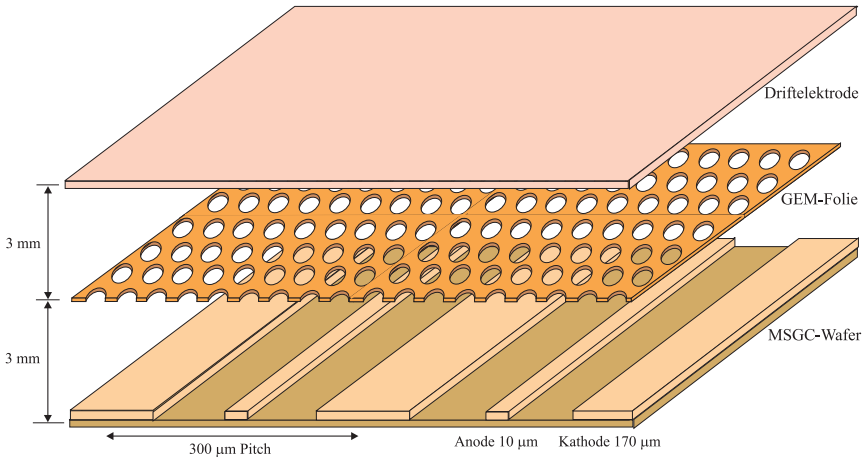

Figure 1: A sketch of the GEM-MSGC detector. The primary ionisation originating from a charged particle passing through the upper gap ('drift gap') is moved by an electrical field to the GEM foil. Due to a large voltage across this foil, gas avalanche multiplication with typically a factor of 30 occurs in the holes of the GEM. The resulting clouds of electrons are now moved through the lower gap ('transfer gap') again by an electrical field of similar size than the drift field. Close to the MSGC anodes a second gas multiplication of typically 100 occurs, regulated by the voltage applied to the MSGC cathodes.

sources or X-ray beams. Therefore a PSI[2] high intensity pion beam (area πM1) has been used to study the chamber characteristics.

The beamline was adjusted to 350 MeV/c, where pions are minimum ionising. Inserting an about 1 mm thick aluminum sheet in front of the last dipol magnet removed most of the protons from the beam. At the place where the chamber was installed, the beam was scanned with a small scintillator (5x5 mm^2) mounted on a table, movable both in x and y direction perpendicular to the beam axis. The beam shape was nearly gaussian with $\sigma_x = 3.3$ cm and $\sigma_y = 4.0$ cm.

The beam intensity could be varied in a large range by changing beam line slits. The total particle rate was determined by a rate measurement in the center of the beam and integration over the gaussian distribution described above.

For the high rate measurements a total particle flux through the chamber of $7 \cdot 10^7$ sec^{-1} was chosen, corresponding to a flux density of 10^4 mm^{-2}sec^{-1} at the beam maximum.

1.2 The GEM-MSGC detector

The GEM-MSGC detector (see figure 1) had an active size of 23 cm x 25 cm. The cover of the chamber consists of a 0.3 mm G10 plate (to ensure mechanical stability) and a 125 μm thick Kapton foil covered with 18 μm copper, which serves as the drift cathode.

The drift gap is 3 mm thick and has a total capacity 200 pF. A vertically incidenting minimum ionising particle produces in Argon (DME) 30 (76) primary ionisation clusters per cm (calculated from [3]). The average size of these clusters was measured in [4] and depends

[2]Paul-Scherrer-Institut, Villigen, Switzerland, http://www.psi.ch/

somewhat on the thickness of the gas gap. For DME no data is available, we use a value of 1.7 measured in CH_4, since it is observed, that many hydrocarbon gases show a similar behaviour in this respect. The value for Argon is 2.4. For our standard Ar/DME 50/50 mixture the mean total primary ionisation charge therefore evaluates to 30 electrons in the 3 mm drift gap. The drift field applied was 5.7 kV/cm resulting in a drift velocity of 5.2 cm/μs [5].

Below the drift gap the GEM foil[3] is mounted. It consists of a 50 μm thick Kapton foil, which is covered with 7 μm copper on each side. The Kapton holes have a diameter of about 55 μm, the corresponding hole diameter in the copper is 95 μm and the holes are staggered with a pitch of 140 μm. An electronically stabilized voltage of 390 V was applied between the upper and the lower surface of the GEM foil. Resistors of 2 MΩ on each side decouple the large cable capacity from the GEM capacity. The total capacity of the GEM was measured to be 30 nF. From laboratory measurements with ^{55}Fe sources and X-ray beams [7] we expect for these conditions a 'visible' gas gain of about 30 in the GEM, determined from the size of the pulses seen at the output of the preamplifier-shaper.

The charge produced in the GEM foil is transfered by an electrical field of about 5.2 kV/cm through the transfer gap of 2.8 mm to a standard MSGC wafer. The wafer is made of 0.4 mm AF45 glass, which was coated by a chemical vapour deposition method ('diamond like')[4]. The coating has a thickness of about 0.08 μm and a typical surface resistance of 10^{14} Ω/square, about two orders of magnitude less than the bulk resistance of the glass. Earlier studies have shown [6] that such a coating remains electrically stable even after strong irradiation, in contrast to the ion conducting DESAG 263 glass used for MSGC's in earlier time, which develops severe local changes in conductivity after irradiation.

A gold layer of 0.5 μm thickness is deposited by vapour onto this wafer and the electrode structure produced by a lift-off technique[5]. This structure consists of 10 μm wide anodes and 170 μm wide cathodes strips, with a gap of 60 μm in between, resulting in a pitch of 300 μm.

16 cathode strips were connected together through a common protection and decoupling resistor of 1 MΩ to 465 Volt, corresponding to an expected visible gas gain on the MSGC wafer of about 100 [7]. At such a low gain cathode-anode discharges ('sparks') due to highly ionising particles as observed for the first time in a beam test in 1996 at PSI [8, 9] and subsequently at HERA–B can be avoided completely.

On the backside the wafer was covered with colloidal graphite to provide a well defined electrical boundary plane both for signal propagation and for the electrostatic field configuration. This backplane is connected with a short wire (few cm length) to the signal reference point of the preamplifier and helps in this way to reduce electrical pickup noise.

The frames which keep the distances between MSGC, GEM and drift cathode consist of G10, have a width of 10 mm and are hollow, thus they act the same time as a gas distribution system.

The chamber was normally operated with Ar/DME 50/50 gas mixture. Some tests with Ar/CO_2 have also been made, but no significant difference in the performance could be observed, with the exception of the stability against α induced sparks on the MSGC, where Ar/DME turns out to be much saver in operation.

[3] produced in the CERN workshop.

[4] coated by Frauenhofer Institute for Surface Engineering and Thin Films, Braunschweig, Germany.

[5] The electrode gold structure is produced by the company IMT in Greifensee, Switzerland, according to masks provided by us.

The detector represents in its active area a total radiation length of $7.8 \cdot 10^{-3}$ (drift cathode $3.2 \cdot 10^{-3}$, GEM foil $1.2 \cdot 10^{-3}$, MSGC wafer $3.4 \cdot 10^{-3}$).

The chamber was mechanically mounted onto a honeycomb plate with polyimid body and carbon fibre skins. This plate is a reasonably good electrical conductor, so it serves as the main grounding point of the system, to which the screening and ground reference of the HV cables and all low voltage power supply references are connected. No further measure against pickup noise was taken.

1.3 Signal coupling and readout electronics

The anodes were connected to the final HELIX 128 readout chip, version 2.2 [11] through a short (3 cm length) Kapton stripline and a fanin, which fits the pitch of the HELIX input pads of 41.4 μm. This fanin is made of thin film ceramics[6] and includes a serial overcurrent protection resistor of 600 Ω to avoid damage of the preamplifier input in case of chamber sparks or shorts. The capacity of the fanin alone was measured to be 2 pF. The capacity from the anodes to the cathodes was measured to be 16 pF. An estimation gives 2.5 pF for the capacity between anode and backplane. The total capacity of the fully mounted system of one anode to the ground is therefore expected to be about 21 pF. The electrical resistance of one anode in its total length was measured to be 1.37 kΩ and the resistance of the cathode 130 Ω.

The signal path is closed through the cathode–backplane capacitance of 180 pF per cathode group and the GEM–cathode capacity of about 200 pF respectively. However since the cathode–anode capacity is in the same order of magnitude (250 pF per group) about half of the cathode signal return current is expected to flow to ground through the neighbouring anodes of the same cathode group. This effect could actually be observed through the normal readout in case of large signals (see figure 3 right).

The HELIX chip is described elsewhere [10] and consists of a charge integrating preamplifier, followed by a shaping stage, which produces a pulse with a FWHM of about 75 ns (foot width 100 ns). The chip includes a 141 stage pipeline (including an 8 fold multi event buffer), a serial readout line and the necessary logic to run the system. The HELIX was run in standard conditions [11], the total signal gain is 85 mV/24000 e^-. This gain decreases[7] to about 50 mV/24000 e^- if the input is connected to a detector with a capacity of 20 pF. The sampling time of the HELIX is given by its 10 MHz clock signal, which was operated independantly of the PSI accelerator clock of 50 MHz. Therefore the sampling time was not optimally set to the pulse maximum, but randomly distributed over 100 ns corresponding to an average reduction of the signal gain of about 1/3.

There was apparently no problem for the HELIX to digest the continuous input current due to the 'diamond' coating of the MSGC of about 36 nA per channel at nominal running condition (Cathode voltage = 465 Volt) and at low signal rates.

The intrinsic noise of the HELIX input amplifier is measured at similar parameter settings to be $445 + 43.6 \cdot C$ electrons equivalent input charge, where C is the capacitance seen at the input given in pF. Since signal propagation in the anode is fast compared to the bandwidth of the amplifier, the full detector capacity C_{anode} has to be taken for a noise estimation.

[6] manufactured by Siegert TFT, Hermsdorf, Thüringen

[7] measured by the Padua group of the ZEUS collaboration, see http://axpze0.pd.infn.it:8080/ZEUS/MVD/shape.html

The 600 Ω protection resistor is expected to give an additional however statistically independant thermal noise of $47.5 \cdot C_{anode}$ electrons (C in pF). Also the finite resistance of the anodes gives a noise contribution of about $100 \cdot C$ electrons, where in this case the relevant value for C is only part of the anode, for a crude estimation[8] we take $C = C_{anode}/2$. These three noise sources have to be added in quadrature, resulting for $C_{anode} = 21$ pF in a total expected thermal noise of about 2000 electrons equivalent input charge (r.m.s.).

2 Measured system performance

Two 5 mm x 5 mm scintillators were mounted 43 cm behind the chamber and were taken in coincidence to trigger the HELIX readout system. On such a trigger signal the analog HELIX data was transfered serially through optical links (length 52 m) to the electronics room, where it was digitised to 8 bit full scale with a resolution of 4 mV/step and subsequently stored to computer disks.

In a first step the correct trigger delay had to be found. While the HELIX ran at a fixed latency of 20 BX (running at 10 MHz), the scintillator trigger delay was varied in steps of 50 ns and the number of channels with signals below -10 ADC counts after baseline subtraction were counted. The resulting delay curve is shown in figure 2. The signals are observed at the value expected from a crude estimation of the various delays involved (including NIM electronics for the scintillator and cable length). The foot width of the distribution of 200 ns is consistent with the expectation from a folding of the width of the HELIX pulse (100 ns) with the BX intervall the HELIX was operated (100 ns).

A more detailed offline analysis shows that from event to event the baseline varies about ±20 ADC channels (80 mV), which is interpreted as correlated pickup noise, since all channels show the same behaviour in parallel. The baseline is therefore determined and subtracted from the data for each event seperately. Furthermore there is a different offset for each single channel, but constant in time, of up to ±10 ADC counts (40 mV) which needs to be subtracted for each channel from the raw data.

Figure 3 shows a typical event, before any corrections are applied. After the corrections signals are identified by applying a threshold. The signal height (largest channel in a cluster) and the cluster width were determined. The resulting pulsheight distribution and the signal positions ('wiremap') are shown in figure 4. The expected intrinsic noise of $\sigma_{noise} = 2000$ e$^-$ would correspond to about 1 ADC count.

A width of the position distribution of 1 cm is expected from the scintillator size of 5 mm and the beam divergence of about 10 mrad. This corresponds to 33 channels, which is compatible with the observation (figure 4 bottom).

The cluster size defined as number of adjacent channels with signal above threshold of 6 counts was found to be 3.4 channels, while the mean width of the clusters (calculated by the sum over the amplitudes of all channels above threshold divided by the size of the largest channel) is 1.9. This observation indicates a somewhat larger cluster size than measured in a similar chamber with similar drift fields in an electron beam in 1997 [12], where the cluster size above threshold was about 2. The beam divergence (estimated to be 10 mrad) and a not exactly perpendicular mounting of the chamber to the beam direction (up to 20 mrad) would explain an increase of the cluster size of at most 0.5 channels.

[8] A SPICE simulation to obtain the correctly predicted total system noise is being performed presently.

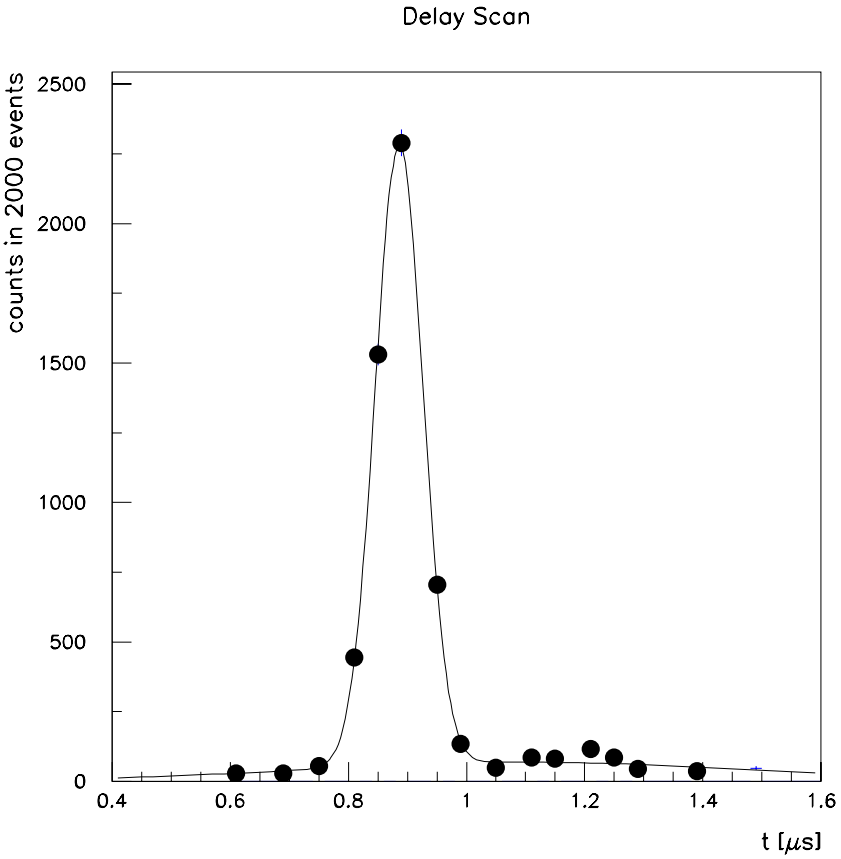

Figure 2: Trigger delay curve of the HELIX readout system showing the number of hits found as a function of the scintillator trigger delay, while the latency in the pipeline of the HELIX was kept constant at 20 BX.

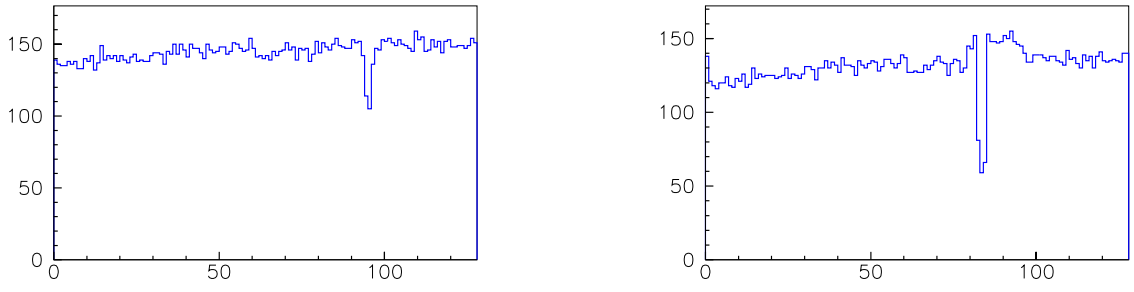

Figure 3: Single event data read out from one HELIX chip, before any corrections applied. Signal size (units = ADC counts) is plotted against anode position. An average size event (left) and a rather large signal (right) is shown. In the latter the inverse current flowing in the neighbouring channels of the same cathode group (channel number 80 to 95) can be identified.

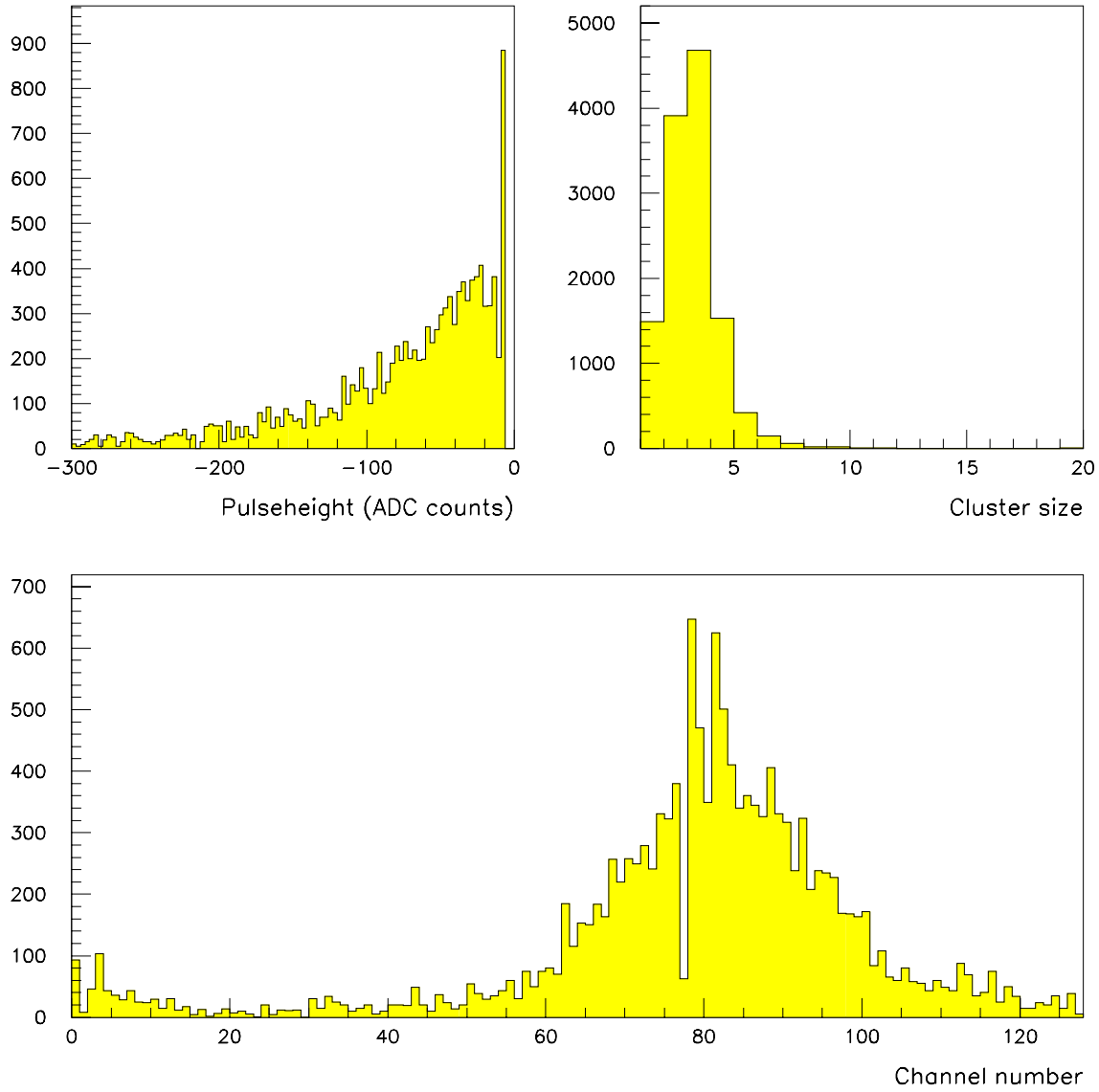

Figure 4: Top left: Pulseheight distribution (sum over all channels of each cluster) in units of ADC counts. The scale shows the true sign; since we observe negative pulses, larger pulses are displayed to the left. The mean value is 76. Top right: Cluster size distribution, i.e. the number of adjacent channels found above threshold for each cluster. Bottom: Position distribution (units = channel number) of identified clusters.

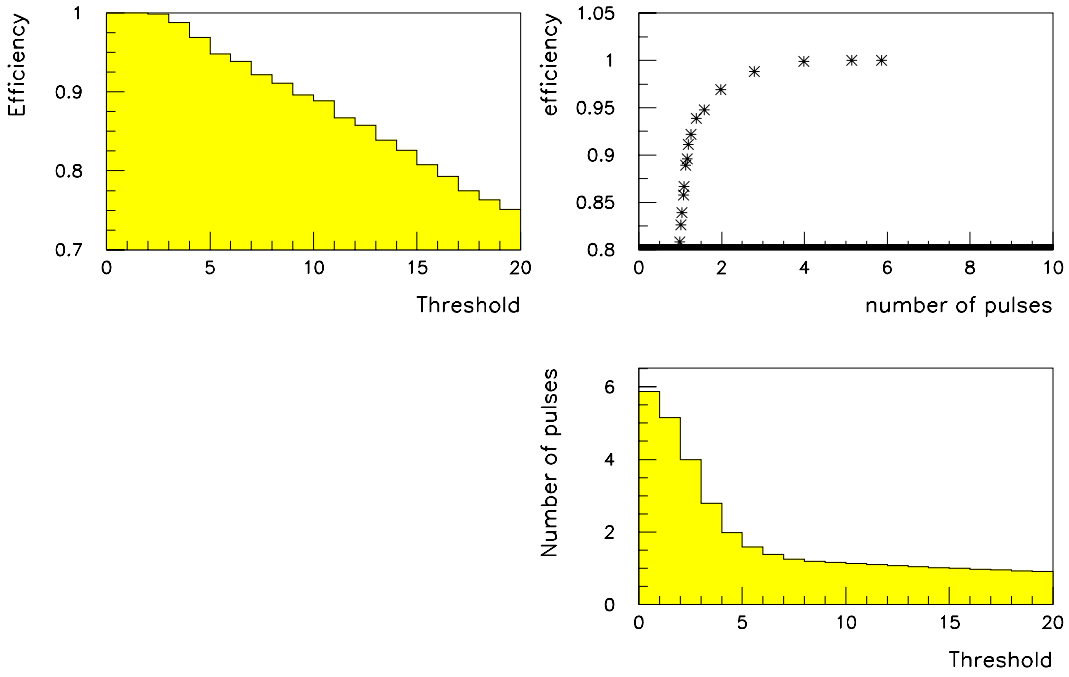

Figure 5: Signal finding efficiency (top left) and number of clusters found in the same chamber region (bottom) as function of the threshold applied (in ADC counts). Top right shows the correlation of these two quantities for different thresholds applied.

For the application in a larger experiment it is relevant to know the efficiency, and how many additional pulses from noise are to be expected, which increase the channel occupancy. The two numbers are obviously correlated through the height of the threshold applied to define a signal. Figure 5 shows the efficiency and number of clusters found as a function of the threshold. If the threshold is set below 5 ADC counts, a significant amount of noise pulses are found. The shape of the noise distribution is somewhat broader than the expected value of 1 ADC count (r.m.s.) from thermal noise. Part of this additional noise can be explained by amplitude variations as a function of the trigger position in the pipeline of the HELIX. Since this position is known for each event one can correct for this effect in principle, but this has not yet been done. In the same figure the correlation between these two quantities is also plotted: For the same data set different thresholds were applied, resulting in different values for efficiencies and noise probabilities. Each point in the plot corresponds to one threshold value. As can be read from the figure running with an efficiency above about 97% results in doubling the occupancy. The absolute value for the efficiency has however a significant systematic uncertainty (few %), since the beam telescope had not yet been setup very carefully.

Summing up all channels above threshold in the signal gives a mean total sum of 76 ADC counts (figure 4 top left), from which we may estimate a total mean charge visible in the readout for a single minimum ionising particle of about 200'000 electrons. Assuming a mean number of 30 primary ionisation electrons this corresponds to a visible gas gain of order 6000, significantly more than we expected so far from X-ray measurements in the lab.

For the measurements discussed so far the total particle illumination of the chamber was chosen to be only about 10 MHz to keep the number of random coincidences small.

The currents into the various electrodes of the system scaled nicely with the particle rate. At a higher rate condition of 70 MHz total flux these currents were measured to be 4.7 μA in the drift cathode, 1.4 and 1.2 μA in the upper and lower GEM surface respectively and 2.1 μA in the cathode (after subtracting the current due the finite resistance of the substrate of 32 μA). From the total sum of these currents divided by the particle flux we can calculate a number of 840'000 ionsation charges per incident minimum ionising particle. Assuming again 30 primary electrons a total 'true' gas amplification of 28'000 can be derived.

Therefore a ratio between 'true' and 'visible' gas gain of about 4 is observed. In an earlier test beam measurement in 1996 [9] with a MSGC setup without GEM using the same gas mixture and comparable preamplifier electronics we found this ratio in the same order of magnitude. This ratio is expected to be about 2 due to the loss of part of the current tail due to the finite integration time of the preamplifier. This value has been observed in high intensity X-ray measurements and it is not inconsistent with a simulation study done within the CMS collaboration ('ballistic deficit')[13], as well as with calculations of our own group.

3 Operation stability

The chamber was run several days under various different beam rates. With the same beam also irradiation of the chamber boundaries (testing the radiation stability of the glued frames etc.) have been performed, where no significant problems occured.

In general the stability of the various currents into the chamber was satisfactory. However small variations of the cathode – anode current due to the 'diamond' coating in the order of a few % were observed.

From time to time a discharge of the GEM foil could be observed through an antisymmetric increase of the two GEM currents for a short period in time. This happened typically every few hours of operation and has been observed in earlier measurements as well. It did not cause any damage to the GEM foil.

However it happened a few times, that such a spark damaged a MSGC anode, although in a beam test in 1997 with similar beam and detector configurations, but lower electrical field in the transfer gap, no such problem was observed. Subsequent laboratory studies show that the probability for a GEM spark to cause damage to the MSGC wafer depends critically on the electrostatic configuration of the system. Further investigations of this problem are going on.

4 Conclusion

For the first time a large GEM-MSGC with the fully pipelined readout system designed for the HERA-B experiment has been operated at high hadronic particle rates. The system showed the expected performance with a relatively large gas amplification. The gas multiplication factor is not understood yet and needs further investigations.

After subtracting correlated pickup signals and channelwise offset values the remaining noise is still somewhat higher than the expected thermal noise of the detector and input stage of the electronics. The correlation of the efficiency with additional occupancy due to noise shows that the operating conditions are realistic for a larger experiment, but there seems to be not too much safety in signal amplitude. The signal size however can be improved by a

correct sample timing. Also since in both the HERA–B and the LHCb spectrometers particle momenta are much larger, the primary ionisation will be higher by 40%.

We thank F. Sauli and his collaborators at CERN for their contribution to the GEM ideas and many other valuable discussions.

References

[1] *HERA-B Technical Design Report*, HERA-B Collaboration, DESY 1994.

[2] *LHCb, Technical Proposal*, LHCb Collaboration,
CERN LHCC 98-4, LHCC/P4, February 20th, 1998.

[3] F. Rieke and W. Prepejchal, Phys. Rev. **A6**, 1507-1519 (1972).

[4] H. Fischle et al., NIM **A301**, 202-214 (1991).

[5] *Electron drift velocities and Townsend coefficents in DME based gas mixtures*,
E. Oettinger, M. Hildebrandt, B. Schmidt, preprint HD-PY-98/01,
to be published in NIM A.

[6] B. Schmidt, *MSGC Development for HERA–B*
http://www.physi.uni-heidelberg.de/groups/herab/text/ERICE_97.ps.gz

[7] Carola Bresch, Diplomarbeit Heidelberg 1997,
http://doc.physi.uni-heidelberg.de/~richter/Diplomarbeit.ps

[8] Sven Visbeck, Diplomarbeit Heidelberg 1996,
http://www.physi.uni-heidelberg.de/groups/herab/text/DiplArb_SVisbeck_light.ps.gz

[9] Tobias Beckmann, Diplomarbeit Heidelberg 1996,
http://www.physi.uni-heidelberg.de/groups/herab/text/DiplArb_TBeckmann.ps.gz

[10] Wolfgang Fallot-Burghardt, Dissertation Heidelberg 1998.

[11] HELIX Manual, http://wwwasic.ihep.uni-heidelberg.de/~feuersta/projects/Helix/helix.ps.gz

[12] Marcus Ziegler, Diplomarbeit Heidelberg 1997,
http://www.physi.uni-heidelberg.de/groups/herab/text/DiplArb_MZiegler.ps.gz

[13] F. G. Sciacca, CMS note 1997/105.